Effects of sterile neutrino and extra-dimension on big bang nucleosynthesis

Dukjae Jang,[1,*] Motohiko Kusakabe,[2,†] and Myung-Ki Cheoun[3,‡]

[1] *Department of Physics and OMEG Institute, Soongsil University, Seoul 156-743, Korea*
[2] *Center for Astrophysics, Department of Physics, University of Notre Dame, Notre Dame, IN 46556, USA*
[3] *Department of Physics, Soongsil University, Seoul 156-743, Korea*

(Dated: November 16, 2016)

By assuming the existence of extra-dimensional sterile neutrinos in big bang nucleosynthesis (BBN) epoch, we investigate the sterile neutrino (ν_s) effects on the BBN and constrain some parameters associated with the ν_s properties. First, for cosmic expansion rate, we take into account effects by a five-dimensional bulk and intrinsic tension of the brane embedded in the bulk, and constrain a key parameter on the extra dimension by the observational element abundances. Second, effects of the ν_s traveling on or off the brane are considered. In this model, the effective mixing angle between the ν_s and an active neutrino depends on energy, which may give rise to a resonance effect on the mixing angle. Consequently, reaction rate of the ν_s can be drastically changed during the cosmic evolution. We estimated abundances and temperature of the ν_s by solving the Boltzmann equation as a function of temperature until the sterile neutrino decoupling and found that the relic abundance of the ν_s is maximized for a characteristic resonance energy $E_{\rm res} \sim 0.4$ GeV. Finally, some constraints related to the ν_s, mixing angle and mass difference, are discussed in detail with the comparison of our BBN calculations corrected by the extra-dimensional ν_s to observational data on light element abundances.

PACS numbers: 14.60.Lm, 26.35.+c

arXiv:1611.04472v1 [nucl-th] 14 Nov 2016

I. INTRODUCTION

Over the past few decades, a considerable number of studies has been conducted on the neutrino oscillation with a great success of measuring neutrino mixing angles. But, some experiments for the neutrino oscillation revealed more or less disagreements with the three-flavor neutrino model, which termed as the neutrino anomalies, as reported in LSND [1], MiniBoone [2], reactor experiments [3] and gallium experiments [4]. One of the approaches for explaining the neutrino anomalies is to presume the existence of the hypothetical fourth neutrino, which is called as sterile neutrino, because the sterile neutrino does not interact with other particles excepting through a mixing with active neutrinos.

Very recently, the IceCube experiment reported a new constrained region for the parameter space of the mixing angle and the mass-squared differences for the 1 eV mass scale sterile neutrino [5], in which the parameter space by previous LSND and MiniBoone data are largely excluded. But, if we recollect that 1 keV cosmological sterile neutrino is still under discussion for a dark matter candidate and the relic neutrino search is being considered, it would be an interesting discussion to consider effects of the sterile neutrino in the big bang nucleosynthesis (BBN) epoch and deduce related parameters from the observational data with the comparison to the IceCube experimental data analysis.

Among many scenarios of the sterile neutrino, Päs *et al.* [6] assumed that the sterile neutrino is a gauge-singlet particle and can travel on or off our 3 + 1 dimensional brane embedded in a large extra dimension bulk similarly to the graviton in the brane-world cosmology. According to the cosmology, ordinary matter fields are confined to a three-dimensional space in the high dimensional bulk. Originally, the brane-world cosmology was suggested to explain the hierarchy problem, the large scale difference between the standard model force and the gravity [7, 8]. Randall and Sundrum suggested a new solution of the hierarchy problem by introducing noncompact extra dimensions [9, 10]. Ref. [6] suggested a model, in which a sterile neutrino can propagate in the bulk space similarly to the graviton. They derived a new formula of resonant active-sterile neutrino oscillation and found an allowed region of the resonance energy from the comparison to available experimental data.

If the production rate of this kind of sterile neutrino is always smaller than the cosmic expansion rate, the abundance of the sterile neutrino never reaches the equilibrium value. The effect of the sterile neutrino on BBN is then completely negligible. This situation has been considered recently [11], and a parameter region where the sterile neutrino abundance is extremely small has been searched by an analytical estimate. However, as shown in this paper, observational constraints on primordial abundances do not exclude the situation that the sterile neutrino is abundantly produced in thermal bath and its abundance attains the equilibrium value in the early universe. Furthermore, the observational abundance of ^{4}He is possibly explained by the effect of the sterile neutrino better than in standard BBN model, as

* havevirtue@ssu.ac.kr
† mkusakab@nd.edu
‡ cheoun@ssu.ac.kr (Corresponding Author)

Typeset by REVTEX

argued in this paper.

In this study, we adopt the same model as Ref. [6] and study effects of a sterile neutrino in an extra-dimensional universe by a numerical BBN calculation in detail. Since the primordial element abundances can be measured with a good precision by the recent great advent of astrophysical spectroscopic observations, the BBN study turns out to be a useful test bed for deriving the cosmological constraints on nonstandard models. For example, some parameters in the modified gravity models, such as $f(R)$ and $f(G)$ gravity, were constrained in detail [12]. In addition, effects of some supersymmetric (SUSY) particles in the early universe have been investigated and parameters, i.e., the lifetime and mass, can be constrained [13].

We include effects of the extra dimensional sterile neutrino in the BBN epoch as follows. The cosmic expansion rate is modified by the large extra dimension [14, 15] as well as the energy density [16, 17] of the sterile neutrino traveling on or off our $3+1$ dimensional brane. Then the modified Friedmann equation and the energy density of decoupled sterile neutrino may change the primordial element abundances. Therefore, the parameters relevant to the extra dimension and the sterile neutrino can be constrained by using observational data of primordial light element abundances.

This paper is composed as follows. In section II, we briefly review the sterile-active neutrino oscillation in the extra-dimension sterile neutrino model and address how to describe the evolution for the number abundance of sterile neutrino in the early universe in the model. In section III, results of primordial nuclear abundances by the model are presented. From the results, in Sec. IV, we discuss the constrained parameter region from the comparison of BBN calculation results to observational abundance data. Section V contains a summary and conclusions of this article.

II. THEORETICAL MODEL

We presume that the universe is five-dimensional and the sterile neutrino travels on or off the five-dimensional space as in Ref. [6]. We simply consider only one sterile neutrino and assume that sterile neutrinos interact with matter particles only via its mixing with an active neutrino. The decay of the sterile neutrino is not considered in this model.

A. Modified cosmic expansion rate from extra-dimension

According to Ref. [18], the cosmic expansion rate in a five-dimensional universe is given by,

$$\begin{aligned}\frac{\dot{a}_0^2}{a_0^2} &= \frac{\kappa^2}{6}\rho_B + \frac{\kappa^4}{36}\rho_b^2 + \frac{\mathcal{E}}{a_0^4} - \frac{K}{a_0^2} \ , \\ &= \frac{\kappa^2}{6}\rho_B + \frac{\kappa^4}{36}\rho_\Lambda^2 + \frac{\kappa^4}{18}\rho_\Lambda\rho + \frac{\kappa^4}{36}\rho^2 + \frac{\mathcal{E}}{a_0^4} - \frac{K}{a_0^2} \ , \end{aligned} \quad (1)$$

where a_0 is the scale factor for the four-dimensional space time. ρ_B denotes the bulk energy density in the universe. Energy density of the brane, ρ_b, is given as a sum of ordinary energy density (ρ) and energy density (ρ_Λ) stemming from the intrinsic tension on the brane, $\rho_b = \rho + \rho_\Lambda$. $\mathcal{E}$ is an integration constant. The five-dimensional analogue of the gravitational constant, $G_{(5)}$, is related to the five-dimensional Planck mass, $M_{(5)}$ and the constant κ, as follows

$$\kappa^2 = 8\pi G_{(5)} = M_{(5)}^{-3} \ . \quad (2)$$

The last term in the right-hand side of Eq. (1) vanishes in the flat universe where the curvature constant is $K = 0$. We can choose ρ_Λ by following Refs. [9, 10]

$$\frac{\kappa^2}{6}\rho_B + \frac{\kappa^4}{36}\rho_\Lambda^2 = 0 \ . \quad (3)$$

Then, the cosmic expansion rate of the standard cosmology is recovered for $\rho \ll \rho_\Lambda$ by the identification [19, 20] of

$$8\pi G \simeq \frac{\kappa^4\rho_\Lambda}{6} \ , \quad (4)$$

where G is Newton's constant. Our final expansion rate was obtained as

$$\frac{\dot{a}^2}{a^2} \simeq \frac{8\pi G}{3}\rho + \frac{\mathcal{E}}{a^4} \ , \quad (5)$$

where the index 0 in the scale factor on the brane a_0 has been omitted.

The first term of the right-hand side in Eq. (5) is identical with the cosmic expansion rate in the standard cosmological model. Note that only the second term comes from the effect of the extra dimension. The free parameter $\mathcal{E}$, which is a kind of an integration constant in the five-dimensional Einstein equation, affects the primordial abundances [14, 15]. The initial temperature of our BBN calculation is $T_9 = T/(10^9\ \mathrm{K}) = 100$ with T the temperature. We then take the value of the second term at $T_9 = 100$, i.e., $\mathcal{E}/a_\mathrm{i}^4$ with a_i the scale factor at the initial temperature, as a parameter.

Figure 1 shows calculated abundances of the deuterium (number ratio of D/H) and ^{4}He (the mass fraction Y_p) as a function of $\mathcal{E}/a_\mathrm{i}^4$. The abundances of D and ^{4}He are monotonically increasing with the increase of $\mathcal{E}/a_\mathrm{i}^4$. The

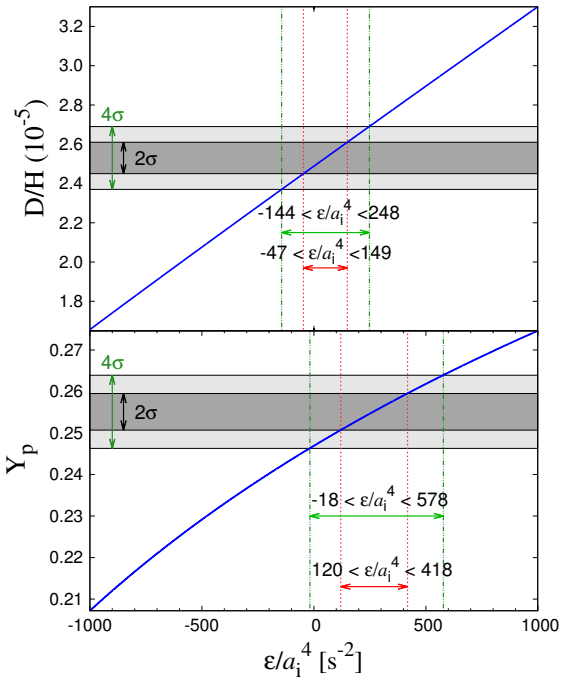

FIG. 1. (Color online) Deuterium (the top panel) and ^{4}He (the bottom panel) abundances as a function of $\mathcal{E}/a_{\rm i}^4$. Shaded and dark-shaded regions are 4 σ and 2 σ ranges, respectively, for the observational primordial abundances. We adopt the observational value of D/H=$(2.53 \pm 0.04) \times 10^{-5}$ [21] and $Y_{\rm p} = (0.2551 \pm 0.0022)$ [22]. From the observational data, the $\mathcal{E}$ value is constrained as $120 < \mathcal{E}/a_{\rm i}^4$ ($\rm s^{-2}$) < 149 (2 σ) and $-18 < \mathcal{E}/a_{\rm i}^4$ ($\rm s^{-2}$) < 248 (4 σ).

standard BBN model corresponds to the case of $\mathcal{E} = 0$. In this case, the predicted deuterium abundance is within the observational 2σ limit, while the ^{4}He abundance is out of the 2σ limit. When the nonzero value of $\mathcal{E}$ is considered, we find the 2σ allowed region from the both D and ^{4}He abundances in the region of $120 < \mathcal{E}/a_{\rm i}^4$ ($\rm s^{-2}$) < 149.

When the $\mathcal{E}$ value is increased, the cosmic expansion rate is also increased. Since the cosmic time scale for a fixed temperature is shorter, the neutron to proton ratio at the ^{4}He synthesis is larger. As a result, the ^{4}He abundance after the BBN is larger. In the late time of BBN, the deuterium is effectively destroyed by the reactions ^{2}H$(d,n)^3$He and ^{2}H$(d,p)^3$H. The shorter cosmic time scale leads to the earlier freeze-out of the destruction reactions. Subsequently, the larger final deuterium abundance is obtained.

B. Relic abundance of sterile neutrino

Since we include the sterile neutrino which has a finite mass $m_{\nu_{\rm s}}$, its energy density $\rho_{\nu_{\rm s}}$ is added to the ordinary density in Eq. (5). The total energy density is thus changed as

$$\rho = \rho_{\rm standard} + \rho_{\nu_{\rm s}} \ , \tag{6}$$

where the first and the second terms indicate energy densities of standard model particles and sterile neutrinos, respectively. The value of $\rho_{\nu_{\rm s}}$ is roughly evaluated as

$$\rho_{\nu_{\rm s}} \simeq \begin{cases} n_{\nu_{\rm s}} \langle E_{\nu_{\rm s}} \rangle & \text{(for relativistic case)} \\ n_{\nu_{\rm s}} m_{\nu_{\rm s}} & \text{(for non-relativistic case).} \end{cases} \tag{7}$$

Here $n_{\nu_{\rm s}}$ and $\langle E_{\nu_{\rm s}} \rangle$ are the number density and the averaged energy of the sterile neutrino, respectively. The energy density is separated into relativistic and non-relativistic cases which depend on temperature $T_{\nu_{\rm s}}$ and $m_{\nu_{\rm s}}$. Namely, for $m_{\nu_{\rm s}} > \langle E_{\nu_{\rm s}} \rangle \sim 3T_{\nu_{\rm s}}$, the sterile neutrino is non-relativistic. Otherwise, it is relativistic. Since the $n_{\nu_{\rm s}}$ in Eq. (7) is a key quantity to determine the energy density of the sterile neutrino, we calculate the number density of the sterile neutrino in the following way.

In the hot early universe, the sterile neutrino is supposed to stay in an equilibrium state. However, with the decrease of temperature, the sterile neutrino is decoupled from the equilibrium state. The decoupling condition is that the reaction rate of the sterile neutrino $\Gamma_{\nu_{\rm s}}$ becomes smaller than the cosmic expansion rate $H \equiv \dot{a}/a$. At that time, the ratio $Y_{\nu_{\rm s}}$ between $n_{\nu_{\rm s}}$ and the entropy density s freezes out, i.e., does not change [23]. In order to describe the $Y_{\nu_{\rm s}}$ evolution, we exploit the following Boltzmann equation

$$\frac{x}{Y_{\rm EQ}} \frac{dY_{\nu_{\rm s}}}{dx} = -\frac{\Gamma_{\nu_{\rm s}}}{H} \left[\left(\frac{Y_{\nu_{\rm s}}}{Y_{\rm EQ}} \right)^2 - 1 \right] , \tag{8}$$

where $x \equiv m_{\nu_{\rm s}}/T$ and $Y_{EQ} = n_{EQ}/s$ is a ratio of the equilibrium number density to the entropy density in the co-moving unit volume given in terms of temperature T

$$s = \frac{2\pi^2}{45} g_{*\rm S} T^3 \ , \tag{9}$$

where $g_{*\rm S}$ is defined in terms of the degrees of freedom of particle i,

$$g_{*\rm S} = \Sigma_{i=\rm boson}\, g_i \left(\frac{T_i}{T} \right)^3 + \frac{7}{8} \Sigma_{i=\rm fermion}\, g_i \left(\frac{T_i}{T} \right)^3 . \tag{10}$$

We note that the temperature of the sterile neutrino is the same as that of thermal bath, i.e., $T_{\nu_{\rm s}} = T$, until the decoupling of the sterile neutrino.

From the assumption that the sterile neutrino interacts with other particles via only mixing, the reaction rate $\Gamma_{\nu_{\rm s}}$ is calculated by a product of interaction strength via mixing and averaged weak interaction rate $\langle \Gamma_{\rm weak} \rangle$ [24, 25]

$$\Gamma_{\nu_{\rm s}} = \frac{1}{2} \sin^2(2\theta) \langle \Gamma_{\rm weak} \rangle \, , \tag{11}$$

where we used the value of $\langle\Gamma_{\rm weak}\rangle = 2.5\,G_{\rm F}^2T^5$ [26]. Note that we assume that the sterile neutrino is in equilibrium state at the initial time. So the initial condition in Eq. (8) is $Y_{\rm i} = Y_{\rm EQ}$. In addition, in Eq. (8), we neglect the effect of an extra-dimension on the cosmic expansion rate. As shown in Sec. II A, observations of light element abundances strongly constrain the value of $\mathcal{E}/a_{\rm i}^4$. The cosmic expansion rate in the early epoch until the sterile neutrino decoupling is, therefore, not allowed to deviate significantly from that in the standard model.

C. Modified mixing probability

There is a further question in solving the Boltzmann equation. The mixing probability in Eq. (11) does not take into account differences between geodesics of a brane and a bulk. Since the trajectories of sterile neutrinos in the bulk and active neutrinos on the brane are different, their mixing probability should be different from that in free space. Time evolution of the sterile and the active neutrinos is described by the following Schrödinger equation, if we ignore the difference between bulk and brane,

$$i\frac{d}{dt}\begin{pmatrix}\nu_a(t)\\ \nu_{\rm s}(t)\end{pmatrix} = H_\nu\begin{pmatrix}\nu_a(t)\\ \nu_{\rm s}(t)\end{pmatrix}. \tag{12}$$

The Hamiltonian in Eq. (12) is

$$H_\nu = E + \frac{1}{2}Tr + \frac{\delta m^2}{4E}\begin{pmatrix}-\cos 2\theta & \sin 2\theta\\ \sin 2\theta & \cos 2\theta\end{pmatrix}, \tag{13}$$

where $Tr = ({m_2}^2 + {m_1}^2)/2E$, $\delta m^2 = {m_2}^2 - {m_1}^2$, θ is a mixing angle between the sterile and active neutrino. E is the energy of the sterile neutrino.

However, if the brane is curved, the effective potential stemming from the difference of trajectories is to be added as follows [6]

$$H_\nu = E + \frac{1}{2}Tr + \frac{\delta m^2}{4E}\begin{pmatrix}-\cos 2\theta & \sin 2\theta\\ \sin 2\theta & \cos 2\theta\end{pmatrix} + \begin{pmatrix}0 & 0\\ 0 & -E\epsilon_s\end{pmatrix}, \tag{14}$$

where $\epsilon_s = (D_b - D_B)/D_b$ is a parameter describing the fractional shortcut difference between geodesics of the bulk D_B and the brane D_b. The last term of the right-hand side in Eq. (14) is analogous to the effective potential in the Mikheev-Smirnov-Wolfenstein (MSW) physics [27, 28].

We note that the matter effect during the BBN is not included in this Hamiltonian. The matter potential is given [11] by $A^{\rm matter}(T) = -3.42\times10^{-20}$ MeV $[T/(1\text{ MeV})]^5(A_a/55.0)$ where A_a is a species-dependent coupling constant of active neutrino. The average potential of the shortcut is, on the other hand, given by $A(T) = -3.151\epsilon_{\rm s}T$. Therefore, the matter potential is negligible with respect to the shortcut potential as long as $\epsilon_{\rm s} \gg 10^{-20}$. Unless the shortcut parameter is extremely small, therefore, the following calculation is applicable.

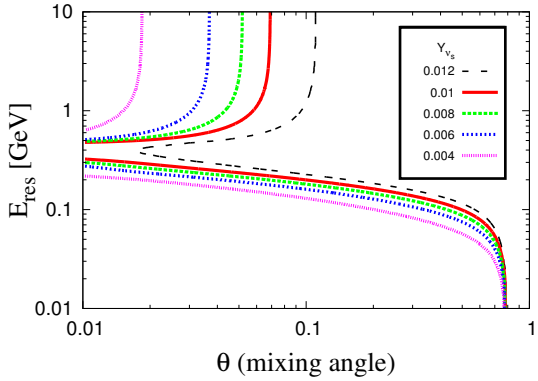

FIG. 2. (Color online) Contours of $Y_{\nu_{\rm s}}$ as a function of θ and $E_{\rm res}$ [GeV].

From the Hamiltonian the modified mixing angle $\tilde{\theta}$ is obtained in terms of the mixing angle θ,

$$\sin^2 2\tilde{\theta} = \frac{\sin^2 2\theta}{\sin^2 2\theta + \cos^2 2\theta[1-(E/E_{\rm res})^2]^2}\,, \tag{15}$$

where $E_{\rm res}$ denotes the resonance energy and can be derived from the condition that two diagonal terms in H_ν are equal to each other,

$$E_{\rm res} = \sqrt{\frac{\delta m^2\cos 2\theta}{2\epsilon_s}}\,. \tag{16}$$

We assume that the sterile neutrino is relativistic before the decoupling. By the assumption, we use the value of $E = 3.151\,T_{\nu_{\rm s}}$, which is the averaged energy for the relativistic fermion with $T_{\nu_{\rm s}}$, the temperature of the sterile neutrino. Finally, the reaction rate $\Gamma_{\nu_{\rm s}}$ modified by the mixing probability is given as

$$\Gamma_{\nu_{\rm s}} = \frac{1}{2}\sin^2\tilde{\theta}\,(2.5G_{\rm F}^2T^5)\,. \tag{17}$$

III. RESULT OF THE BOLTZMANN EQUATION

By using the modified mixing probability, we calculate the Boltzmann equation in the temperature interval of 100 GeV $\geq T \geq$ 10 MeV. Figure 2 shows the contours of $Y_{\nu_{\rm s}}$ as a function of θ and $E_{\rm res}$. Here the sterile neutrino energy is set to be $E = 3.151T_{\nu_{\rm s}}$. We discuss the result from three viewpoints.

A. Mixing angle vs. $Y_{\nu_{\rm s}}$

First, we explain the results in Fig. 2 as a function of mixing angle for a given $E_{\rm res}$. The value of $Y_{\nu_{\rm s}}$ becomes larger for larger mixing angle simply because the larger

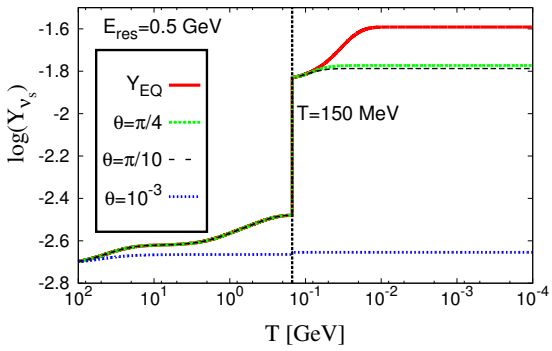

FIG. 3. (Color online) Temperature evolution of the abundance of sterile neutrino derived by solving the Boltzmann equation. The red-solid line indicates the equilibrium abundance $Y_{\rm EQ}$ and other lines show the abundance of the sterile neutrino $Y_{\nu_{\rm s}}$ for the mixing angle $\theta = \pi/4$ (higher dashed line), $\pi/10$ (lower dashed line), and 0.001 (dotted line), respectively. In this figure, the resonance energy is fixed as 0.5 GeV for example. Also, black vertical dashed line at $T = 150\,{\rm MeV}$ shows the temperature of the quark-hadron transition. At the temperature, the equilibrium abundance of the sterile neutrino is rapidly increased because of decreasing $g_{*\rm S}$.

mixing angle increases the reaction rate of the sterile neutrino. This can be easily understood in Eqs. (15) and (17), in which the larger mixing angle produces the larger mixing probability and reaction rate.

We note that the abundance $Y_{\nu_{\rm s}}$ is increased with decreasing T because the number of degrees of freedom $g_{*\rm S}$ decreases. This behavior is remarkably contrary to the decrease of $Y_{\nu_{\rm s}}$ by the exponential decrease of the equilibrium number density $n_{\rm EQ}$ after the sterile neutrino becomes non-relativistic. Because of the hadronization of the quark-gluon plasma (QGP) the abundance $Y_{\nu_{\rm s}}$ is increased with decreasing temperature in this epoch. This feature can be seen in Fig. 3. In this figure, the entropy density is calculated by a standard method [23] described in Ref. [29].

In the early universe, particles are decoupled from the equilibrium state when the reaction rate Γ is smaller than the cosmic expansion rate H. Therefore, the sterile neutrino is decoupled at a temperature when the reaction rate of the sterile neutrino becomes relatively small. The number of degrees of freedom for the entropy $g_{*\rm S}$ in Eq. (10) is decreased at the lower temperature [29]. The freeze-out abundance $Y_{\nu_{\rm s}}$ then becomes larger for larger mixing angle because the freeze-out occurs later. This dependence on θ is valid for any resonance energy parameters.

B. The resonance energy vs. $Y_{\nu_{\rm s}}$

Second, the resonance energy dependence is interpreted similarly, because it is related to the reaction rate of the sterile neutrino. Figure 4 shows the temperature evolution of effective mixing angle, $\sin^2 2\tilde{\theta}$ (the top panel), and $Y_{\nu_{\rm s}}$ (the bottom panel). The value of mixing angle θ is fixed as 0.03. The black vertical dashed line at $T = 150\,{\rm MeV}$ corresponds to the temperature of the quark-hadron transition. At the temperature, the equilibrium abundance of the sterile neutrino is increased because of decreasing $g_{*\rm S}$. For the case of $E_{\rm res} = 0.05\,{\rm GeV}$, the resonance peak occurs at $T < 150\,{\rm MeV}$ and the reaction rate of the sterile neutrino is small at early time. Because the reaction rate becomes smaller than the cosmic expansion rate at the early time, it freezes out earlier and its final abundance is small. On the other hand, for the case of $E_{\rm res} = 0.4\,{\rm GeV}$, the resonance peak occurs at around $T = 150\,{\rm MeV}$. For this reason, the reaction rates is the highest at $T \sim 150\,{\rm MeV}$ and after this point, the reaction rate is decreased. So the sterile neutrino is decoupled at $T < 150\,{\rm MeV}$ and its final abundance is large. In the case of $E_{\rm res} = 3\,{\rm GeV}$, reaction rates are high in the early time. However, the resonance peak occurs at $T > 150\,{\rm MeV}$ and the reaction rate is decreased before $T = 150\,{\rm MeV}$. Therefore, although the decoupling occurs later than that of $E_{\rm res} = 0.05\,{\rm GeV}$, it is earlier than that of $E_{\rm res} = 0.4\,{\rm GeV}$. The final abundance is then higher than that of $E_{\rm res} = 0.05\,{\rm GeV}$ but smaller than that of $E_{\rm res} = 0.4\,{\rm GeV}$.

We can discuss the dependence of the final abundance on the parameter $E_{\rm res}$ in the following three regions. The first region is $E_{\rm res} \lesssim T_{\rm dec}$, where $T_{\rm dec}$ is the decoupling temperature of the sterile neutrino which depends on the parameter $E_{\rm res}$ and θ. In this region, the final abundance of the sterile neutrino $Y_{\nu_{\rm s}}$ is increased with the increase of the resonance energy at the same mixing angle because the reaction rate is increased as shown in Eq. (15).

The second region is resonance region, *i.e.*, $E_{\rm res} \sim T_{\rm dec}$, in which the resonance condition gives the highest mixing probability in the decoupling epoch. Consequently the highest value of $Y_{\nu_{\rm s}}$ is realized in the region. The third region is $E_{\rm res} \gtrsim T_{\rm dec}$. The dependence is similar to the case for $E_{\rm res} \lesssim T_{\rm dec}$ [Eq. (15)]. However, if the resonance energy is much larger than $T_{\rm dec}$, the dependence on the resonance energy disappears and the value of $Y_{\nu_{\rm s}}$ depends only on the mixing angle.

C. Decoupling temperature

Finally, we discuss $\nu_{\rm s}$ decoupling temperature in order to describe time evolution of energy density of the sterile neutrino during BBN. First, we define a parameter

$$r_s = \frac{T_{\nu_{\rm s}}}{T_\nu}, \tag{18}$$

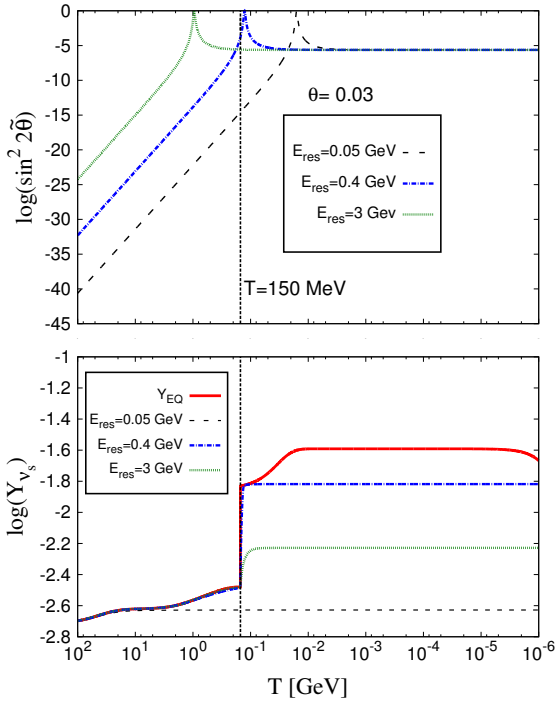

FIG. 4. (Color online) Temperature evolution of the abundance and the effective mixing angle of the sterile neutrino derived by Botlzmann equation. The value of mixing angle is fixed as 0.03. The red solid line indicates the equilibrium abundances $Y_{\rm EQ}$ and other lines show the abundance of the sterile neutrino $Y_{\nu_{\rm s}}$ for the resonance energy $E_{\rm res} = 0.05\,{\rm GeV}$ (long dashed line), $0.4\,{\rm GeV}$ (dashed-dotted line) and $3\,{\rm GeV}$ (dotted line).

where $T_{\nu_{\rm s}}$ and T_ν are temperatures of sterile neutrino and active neutrinos, respectively, for a fixed cosmic time. This ratio is unity before the decoupling of the sterile neutrino. After the decoupling, the temperatures can be different, and the ratio is smaller than 1, in general. After active neutrino decoupling, the two temperatures have the same scaling with a scale factor of the universe. The ratio is, therefore, kept constant again.

The $r_{\rm s}$ value after the decoupling is given by

$$r_s = \frac{T_{\nu_{\rm s}}}{T_\nu} = \left(\frac{g_{*\rm S}}{g_{*\rm S,dec}}\right)^{1/3}, \qquad (19)$$

where $g_{*\rm S}$ and $g_{*\rm S,dec}$ denote the relativistic degrees of freedom, which does not contain the contribution of the sterile neutrino, at the decoupling temperature of active and sterile neutrinos, respectively. The second equality is derived from the evolution of the active neutrino temperature by taking into account the entropy conservation [23].

This ratio is found to be constant between the initial temperature of BBN calculation, which is taken to be $T_9 = 100$, and the active neutrino decoupling temperature $T_9 \sim 10$, due to the following reason. In this temperature interval, numbers of degree of freedom for entropy

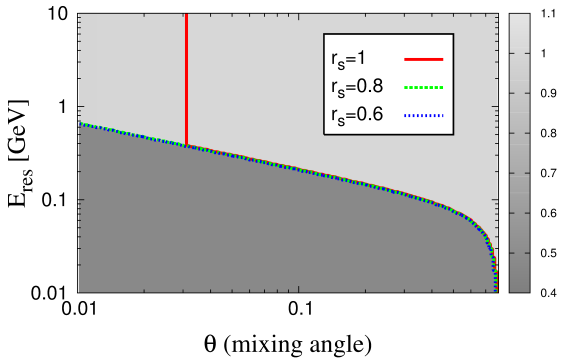

FIG. 5. (Color online) Contours of $r_{\rm s}$ in the parameter plane of θ and $E_{\rm res}$ [GeV]. Note that there is a phase transition of $r_{\rm s}$ between a light-shaded and a dark-shaded region, where both shaded regions have a specific constant $r_{\rm s}$ value. We denote results at special cases of $r_s = 1$, 0.8 and 0.6 as different colors, most of which are located in the uppermost shaded region.

does not change. Therefore, both temperatures of the sterile and active neutrinos simply scale as $T \propto 1/a$. We then use this constant ratio in the BBN calculation.

Figure 5 shows calculated ratio $r_{\rm s}$ in the parameter plane of θ and $E_{\rm res}$. This ratio r_s depends on θ and $E_{\rm res}$ since the decoupling temperature of the sterile neutrino depends on its reaction rate determined by those parameters. The ratio is rapidly increased at a curved line. Above the line the sterile neutrinos decouple after the quark-hadron transition, while below the line they decouple before the transition. If the transition occurred, then the degrees of freedom is rapidly decreased. Therefore $g_{*\rm S}$ is rapidly decreased and the $r_{\rm s}$ is rapidly increased according to Eq. (19). In this calculation, we assumed that the quark-hadron transition occurred at $T = 150\,{\rm MeV}$ [31]. Therefore, the transition affects the energy density of the sterile neutrino through the $r_{\rm s}$ parameter determining the averaged energy of the sterile neutrino during BBN epoch.

IV. RESULTS OF BBN

From the Boltzmann equation, final abundances and energy density of the sterile neutrino are determined. Then the cosmic expansion rate is modified as follows

$$H^2 = \frac{8\pi G}{3}(\rho_{\rm standard} + \rho_{\nu_{\rm s}}) + \frac{\mathcal{E}}{a^4}. \qquad (20)$$

The modified expansion rate would change primordial abundances. We can then constrain the relevant parameters, θ, $E_{\rm res}$, $m_{\nu_{\rm s}}$ and $\mathcal{E}$, by comparing calculated abundances to the observational data. We expect that the primordial elemental abundances depend on the sterile neutrino abundance, $Y_{\nu_{\rm s}}$ shown in Fig. 2 because the

cosmic expansion rate depends on the energy density of the sterile neutrino.

A. BBN Calculation and Observational Constraints

We use updated reaction rates [32, 33] in the BBN calculation code [34, 35]. The neutron lifetime is taken from the central value of the Particle Data Group, 880.3± 1.1 s [36]. The baryon-to-photon ratio is adopted from the value $\eta = (6.037 \pm 0.077) \times 10^{-10}$ corresponding to the baryon density in the base ΛCDM model (Planck+WP) determined from Planck observation of cosmic microwave background, $\Omega_{\rm m} h^2 = 0.02205 \pm 0.00028$ [37].

The primordial D abundance comes from observations of quasistellar object (QSO) absorption systems and its value is D/H=$(2.53 \pm 0.04) \times 10^{-5}$. We take 2σ limit $(2.53 \pm 0.08) \times 10^{-5}$ and 4σ limit $(2.53 \pm 0.16) \times 10^{-5}$ in the following analysis. For ^{4}He, we adopt $Y_p = 0.2551 \pm 0.0022$ which is observed from metal-poor extragalactic HII region [21] and also consider their 2σ limit (0.2551 ± 0.0044) and 4σ limit (0.2551 ± 0.0088).

B. $\mathcal{E} = 0$ and $m_{\nu_{\rm s}} = 1\,{\rm keV}$

Figure 6 shows the result of the primordial abundance in the case of $\mathcal{E} = 0$ and $m_{\nu_{\rm s}} = 1$keV. Since $\mathcal{E}$ is equal to zero, only the energy density of the sterile neutrino affects the cosmic expansion rate. Since the mass of the sterile neutrino is 1 keV, it is relativistic during BBN epoch. For deuterium abundance, all parameter regions adopted here are allowed by the 2 σ limit. We find a parameter region in which the calculated ^{4}He abundances satisfy the observational 2σ constraints. This allowed region is not seen in the standard BBN result (see Fig. 1 at $\mathcal{E}/a_{\rm i}^4 = 0$). The existence of the sterile neutrino energy density, however, increases the cosmic expansion rate, and as a result, abundances of D and ^{4}He are increased. All parameter regions are allowed by the 4σ limit.

The shapes of contours can be interpreted as follows. The energy density scales as

$$\rho_{\nu_{\rm s}} = n_{\nu_{\rm s}} \langle E_{\nu_{\rm s}} \rangle \propto Y_{\nu_{\rm s}} T_{\nu_{\rm s}} \propto Y_{\nu_{\rm s}} r_{\rm s}. \quad (21)$$

The number abundance of sterile neutrino is proportional to $Y_{\nu_{\rm s}}$ shown in Fig. 2. The abundance is then high in the large θ region, and there is a narrow peak at $E_{\rm res} = \mathcal{O}(0.1)$ GeV. This dependence is appearing again in Fig. 6. Since the energy density of sterile neutrino becomes larger for the larger θ values and the critical resonance energy of $E_{\rm res} = \mathcal{O}(0.1)$ GeV, the abundances of D and ^{4}He are increased in the right upper region of Fig. 6. Also, the energy density is proportional to the sterile neutrino temperature or $r_{\rm s}$ shown in Fig. 5. There is a rapid change of the $r_{\rm s}$ value related to whether the sterile neutrino decoupling occurs before or after the quark hadron transition. In the upper region from this boundary of high and low $r_{\rm s}$ regions in Fig. 5, the energy density is large. The abundances of D and ^{4}He are then larger above the boundary. The contours in Fig. 6 thus result from such a combined effect of the abundance and the temperature of the sterile neutrino.

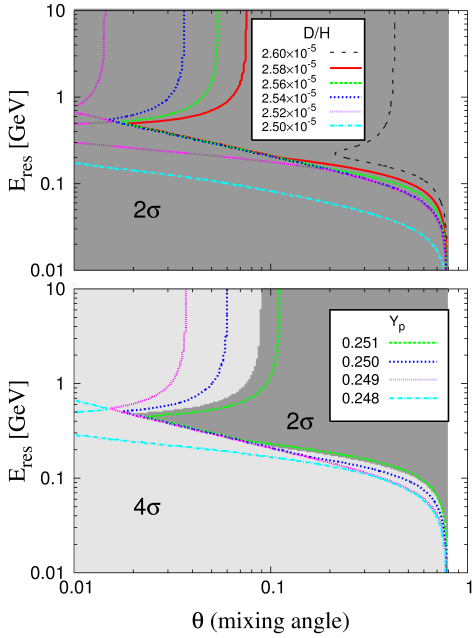

FIG. 6. (Color online) Contours of deuterium abundance (the top panel) and ^{4}He abundance (the bottom panel) in the parameter plane of θ and $E_{\rm res}$ [GeV] for the case of $m_{\nu_{\rm s}} = 1\,{\rm keV}$ and $\mathcal{E} = 0$. Parameter ranges are $0.01 \le \theta \le \pi/4$ and $0.01\,{\rm GeV} \le E_{\rm res} \le 10\,{\rm GeV}$, respectively. Dark-shaded and shaded color regions are 2 σ and 4 σ allowed regions, respectively.

C. Constraint on $\mathcal{E}$

First, we consider the case of the smallest number abundance of the sterile neutrino realized in the parameter region. Figure 7 shows the calculated abundances of deuterium and ^{4}He, and also constraints on $\mathcal{E}$ similar to those in Fig. 1. The mass of the sterile neutrino $m_{\nu_{\rm s}}$ is assumed as 1 eV which was the mass scale discussed in the reactor anomalies. Mixing angle θ and resonance energy $E_{\rm res}$ are fixed to be 0.01 radian and 0.01 GeV, respectively. From the Boltzmann equation result, these values give the lowest reaction rate of the sterile neutrino, that is, the smallest relic number abundance of the sterile neutrino. Since the sterile neutrino increases the cosmic expansion rate, constrained values of $\mathcal{E}$ are shifted to the left side compared to those of Fig. 1. Namely, $120 < \mathcal{E}/a_{\rm i}^4\ ({\rm s}^{-2}) < 149$ (2σ) and $-18 < \mathcal{E}/a_{\rm i}^4\ ({\rm s}^{-2}) <$

248 (4σ) regions are shifted to $108 < \mathcal{E}/a_{\rm i}^4$ (s^{-2}) < 139 (2σ) and $-30 < \mathcal{E}/a_{\rm i}^4$ (s^{-2}) < 237 (4σ), respectively. Therefore, Fig. 7 shows that some parameter regions of $139 < \mathcal{E}/a_{\rm i}^4$ (s^{-2}) < 149 (2σ allowed region in Fig. 1) and $237 < \mathcal{E}/a_{\rm i}^4$ (s^{-2}) < 248 (4σ) are excluded by the sterile neutrino assumed to be existent in BBN epoch.

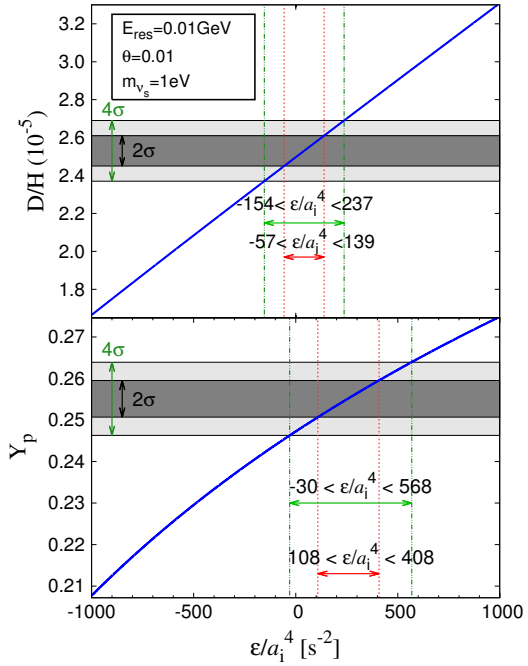

FIG. 7. Same as Fig. 1. But here we include the sterile neutrino which has $m_{\nu_{\rm s}} = 1$eV, $\theta = 0.01$ and $E_{\rm res} = 0.01$GeV. The value of $\mathcal{E}$ is constrained as $108 < \mathcal{E}/a_{\rm i}^4$ (s^{-2}) < 139 and $-30 < \mathcal{E}/a_{\rm i}^4$ (s^{-2}) < 237 by the 2σ and 4σ limit, respectively.

Fig. 8 shows the contours for the case of $\mathcal{E}/a_{\rm i}^4 = 248$ s^{-2} and $m_{\nu_{\rm s}} = 1\,$eV. Although the highest value for the 4 σ allowed region in Fig. 1, i.e., $\mathcal{E}/a_{\rm i}^4 = 248$ s^{-2}, is adopted in Fig. 1, it is excluded by the over-abundance of deuterium when the 1 eV sterile neutrino is added.

D. Constraint on the mass

Figure 9 shows the primordial abundances as a function of $\delta m^2 \equiv m_{\nu_{\rm s}}^2 - m_{\nu_a}^2$ in the same condition of Fig. 7, where the parameters θ and $E_{\rm res}$ are adopted to be 0.01 radian and 0.01 GeV, respectively. The value of $\mathcal{E}$ is fixed by the lowest value of the 2 σ and 4σ allowed value derived for the case without the sterile neutrino. Because of $m_{\nu_a} \ll 1\,$eV, we neglected the mass of the active neutrino. Thus, δm^2 is approximately the same as the squared mass of the sterile neutrino. For $\delta m^2 \lesssim 10^{-9}\,$GeV^2, there is no contribution of the sterile neutrino mass because the sterile neutrino is relativistic during the BBN epoch. If the sterile neutrino is relativistic in the BBN epoch, then the cosmic expansion rate does not depend on the mass of the sterile neutrino but only its number density.

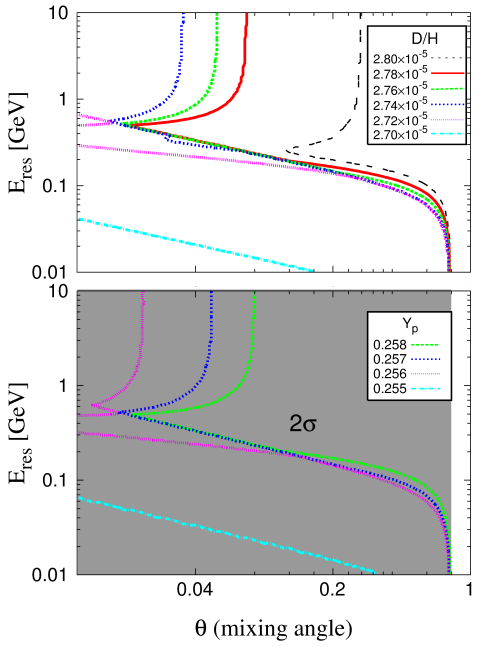

FIG. 8. (Color online) Same as Fig. 6, but for $\mathcal{E}/a_{\rm i}^4 = 248$ s^{-2} and $m_{\nu_{\rm s}} = 1\,$eV. All parameter regions are excluded by the constraint on D/H while whole regions are allowed by that on Y_p at 2σ level.

However, if $m_{\nu_{\rm s}}$ gets larger, then the sterile neutrino would be non-relativistic and its mass affects the cosmic expansion rate. As a result, for the lowest value $\mathcal{E}/a_{\rm i}^4 = -18$ s^{-2} in the 4σ limit, δm^2 is allowed up to $9 \times 10^{-7}\,$GeV^2 and $2 \times 10^{-6}\,$GeV^2 by the 2σ and 4σ limits, respectively. For another lowest value $\mathcal{E}/a_{\rm i}^4 = 120$ s^{-2} from the 2σ limit, δm^2 is allowed up to $2\times10^{-8}\,$GeV^2 and $5 \times 10^{-7}\,$GeV^2 by the 2σ and 4σ limits, respectively. The results mean that sterile neutrinos which have masses larger than the order of 1 MeV are excluded by this BBN constraint.

Figure 10 shows the same contours of light element abundances as in Fig. 6 for the case of 1 MeV sterile neutrino and $\mathcal{E}/a_{\rm i}^4 = -20$ s^{-2}, for example. This value of $\mathcal{E}/a_{\rm i}^4 = -20$ s^{-2} is near the lowest allowed value in Fig. 1 for the $4\,\sigma$ limit. In this case, all parameter regions are excluded by the over-abundance of deuterium at the observational 2σ level. For the 4σ limit case, the left-bottom side of the parameter region is allowed.

In the present model of a sterile neutrino, the effective mixing angle depends on the energy by Eq. (15). Results of neutrino experiments, therefore, do not always exclude the parameter region for large values of θ. For example, if we assume the resonance energy $E_{\rm res} = 400$ MeV (corresponding to Figure 4 in Ref. [6]), for the energy region of the IceCube measurement [5], i.e., 320 GeV

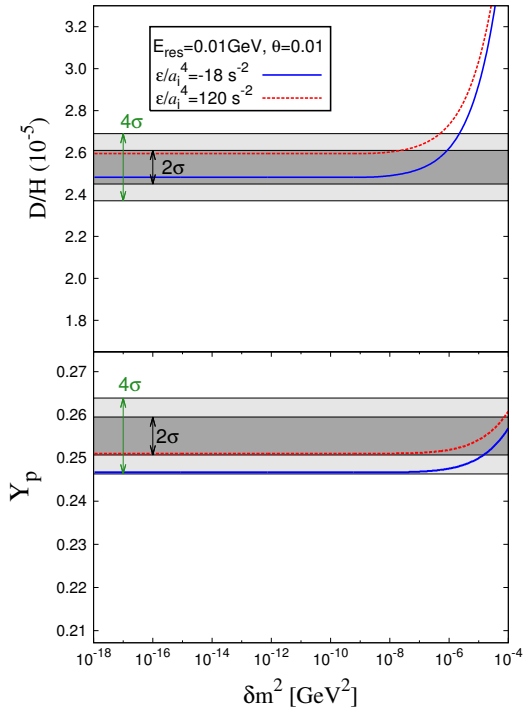

FIG. 9. (Color online) Primordial abundances of D and ^{4}He as a function of δm^2. The parameters θ and $E_{\rm res}$ are fixed at 0.01 radian and 0.01 GeV, respectively. The dotted red and the solid blue line denote the abundances for $\mathcal{E}/a_{\rm i}^4 = 120$ and -18 s^{-2}, respectively. The limits from observed abundances are delineated by the horizontal lines: inner lines (2σ) and outer lines (4σ).

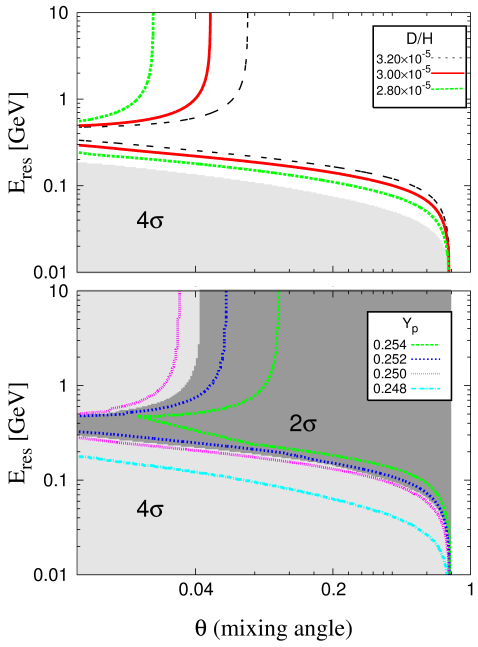

FIG. 10. (Color online) Same as Fig. 6, but for $m_{\nu_{\rm s}} = 1$MeV and $\mathcal{E}/a_{\rm i}^4 = -20$ s^{-2}.

~ 20 TeV, the effective mixing angle becomes negligibly small. The IceCube data, therefore, are consistent with this model, independently of the mixing angle θ. The experimental verification of the mixing of a sterile neutrino, which propagates to the bulk space, then requires measurements of the effective mixing angle for various neutrino energies.

E. Dependence of primordial abundances on δm^2 and θ

Figure 11 shows the primordial abundances as a function of δm^2 and the mixing angle θ. The values of $\mathcal{E}$ and $E_{\rm res}$ are fixed, respectively, at 0 and 0.3 GeV. If δm^2 is larger than $10^{-8}\,{\rm GeV}^2$, then the primordial abundances are increased because the cosmic expansion rate depends on the mass of the sterile neutrino by Eq. (7). In the high mass region of the figure, deuterium and ^{4}He abundances are high. The mixing angle, meanwhile, is related to the reaction rate of sterile neutrino. If the mixing angle is increased, therefore, the reaction rate of the sterile neutrino is also increased and it makes higher number- and energy-densities of the sterile neutrino. Therefore, final abundances of light elements become higher by increasing the mixing angle θ similarly to the previous contour plot of Fig. 10. If the δm^2 value is higher than $10^{-7}{\rm GeV}^2$, the region is excluded by over-production of the deuterium.

F. Dependence of primordial abundances on δm^2 and $E_{\rm res}$

Figure 12 shows the primordial abundances as a function of δm^2 and $E_{\rm res}$. The value of $\mathcal{E}$ and θ are fixed, respectively, at 0 and 0.03. In the figure, the tendency of the δm^2 is similar to Fig. 11 by the same reason. The curved shape for the parameter $E_{\rm res}$ appears by the reason that the number abundance of the sterile neutrino is the highest when the resonance energy is equal to the energy of the sterile neutrino during its decoupling epoch. Then the higher number abundance of sterile neutrino around $E_{\rm res} \simeq 0.3\,{\rm GeV}$ makes the larger energy density and it affects the cosmic expansion rate more. This gives higher primordial abundances. The curved shape pattern is then similar to the pattern of Fig. 2. The region of $\delta m^2 \geq 10^{-7}\,{\rm GeV}^2$ is excluded by the over-production of deuterium, also in this case.

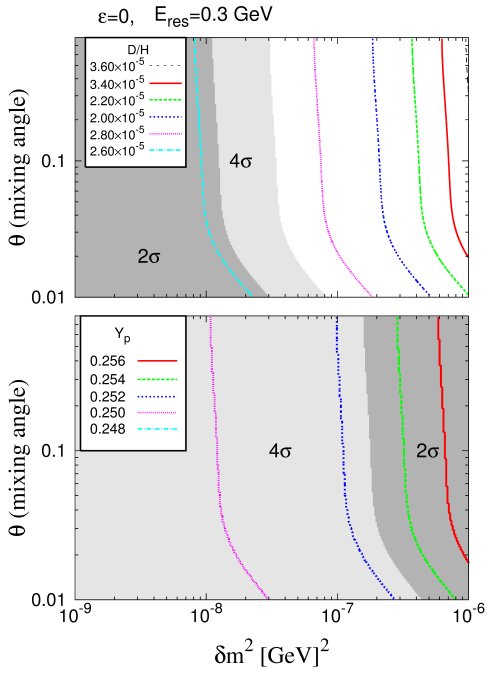

FIG. 11. (Color online) Contours of deuterium abundance (the top panel) and ^{4}He abundance (the bottom panel) in the parameter plane of θ and δm^2 [GeV^2] for the case of $\mathcal{E} = 0$ and $E_{\rm res} = 0.3\,{\rm GeV}$. Parameter ranges are $0.01 \leq \theta \leq \pi/4$ and $1.0\times10^{-9}\,{\rm GeV}^2 \leq \delta m^2 \leq 1.5\times10^{-6}\,{\rm GeV}^2$. Dark-shaded and shaded regions are 2σ and 4σ allowed regions, respectively.

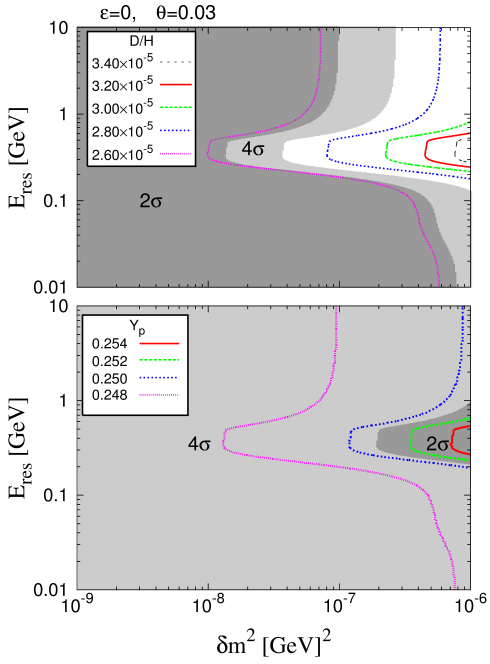

FIG. 12. (Color online) Contours of deuterium abundance (the top panel) and ^{4}He abundance (the bottom panel) in the parameter plane of $E_{\rm res}$ and δm^2 [GeV^2] for the case of $\mathcal{E} = 0$ and $\theta = 0.03$. Parameter ranges are $0.01\,{\rm GeV} \leq {\rm E_{res}} \leq 10\,{\rm GeV}$ and $1.0\times10^{-8}\,{\rm GeV}^2 \leq \delta m^2 \leq 1.5\times10^{-6}\,{\rm GeV}^2$. Dark-shaded and shaded color regions are 2σ and 4σ allowed regions, respectively.

V. CONCLUSION

In this work, we study effects of a sterile neutrino which can propagate to the bulk space in the five dimensional universe on BBN. In the present model, the cosmic expansion rate is modified by the energy density of the sterile neutrino and the existence of the fifth dimension itself. We then deduce parameter regions relevant to the multi-dimensional sterile neutrino by using results of the BBN calculation. The five-dimensional effect is described by one parameter $\mathcal{E}$, and the energy density of the sterile neutrino depends on three parameters, i.e., $E_{\rm res}$, θ and $m_{\nu_{\rm s}}$. This model therefore has four physical parameters. Two of them are integration constants: (1) $\mathcal{E}$ comes from the integration of five-dimensional Einstein equation and (2) ϵ_s describing the shortcut, i.e., the difference of geodesics in the bulk and on the brane in five dimensional cosmology. The latter is reflected in the sterile neutrino resonance energy $E_{\rm res}$ in Eq. (16). The other two parameters are mixing angle and mass scale of the sterile neutrino. These four parameters modify the cosmic expansion rate and the matter density in the BBN epoch. Taking into account the modified cosmic expansion rate, we investigated how primordial abundances are changed and constrained the parameters using the observational abundance data.

First, the parameter $\mathcal{E}$ manifests itself in the cosmic expansion rate and influences the primordial abundances. When we do not consider the sterile neutrino, then $\mathcal{E}$ is constrained by the observed abundances : $120 < \mathcal{E}/a_{\rm i}^4\ ({\rm s}^{-2}) < 149$ and $-18 < \mathcal{E}/a_{\rm i}^4\ ({\rm s}^{-2}) < 248$ from the observational 2 σ and 4 σ limits, respectively. However, if the sterile neutrino is included, the cosmic expansion rate is increased and high $\mathcal{E}$ values are excluded. For example, we observed that the constraints are shifted to $108 < \mathcal{E}/a_{\rm i}^4\ ({\rm s}^{-2}) < 139$ (2σ) and $-30 < \mathcal{E}/a_{\rm i}^4\ ({\rm s}^{-2}) < 237$ (4σ) in the case of $m_{\nu_{\rm s}} = 1$ eV, $\theta = 0.01$ and $E_{\rm res} = 0.01$ GeV (Fig. 7).

Second, we took into account the effect of the energy density of the sterile neutrino which can propagate in the bulk space. The relic abundance and the temperature of the sterile neutrino are calculated by solving the Boltzmann equation. The energy density of the sterile neutrino depends on not only the mass but also the number density and the temperature. Since the mixing angle and the resonance energy are related to the reaction rate of the sterile neutrino, the two parameters determine the relic abundance of the sterile neutrino. The parameters are then constrained through the comparison of the BBN calculation results and observed elemental abundances. The final abundance of the sterile neutrino is increased

when the sterile neutrino has a large reaction rate. Especially, if the sterile neutrino is decoupled after the quark-hadron transition, then the number density of the sterile neutrino is rapidly increased.

We found that the relic abundance is large for large values of θ and a characteristic resonance energy $E_{\rm res} \sim 0.4$ GeV (Fig. 2). This value of resonance energy corresponds to the average energy at the quark hadron transition $T \sim 150$ MeV. The ratio of the temperatures of the sterile and active neutrinos, $r_{\rm S}$, after the decoupling of the active neutrino depends on the decoupling temperature of the sterile neutrino. The decoupling temperature is determined by the parameters θ and $E_{\rm res}$. It is found that the ratio significantly changes depending on whether the decoupling occurs before or after the quark hadron transition (Fig. 5).

When the sterile neutrino is relativistic during BBN, the energy density of the sterile neutrino is determined by the relic abundance $Y_{\nu_{\rm s}}$ and the temperature ratio $r_{\rm S}$. The energy density is larger for a sterile neutrino which decouples later since its abundance and the temperature ratio are larger. We then derived a constraint on the parameters for the case of $\mathcal{E} = 0$ (Fig. 6). If the mass of the sterile neutrino is larger than $\sim$1 MeV, then it becomes non-relativistic in the BBN epoch. So the energy density of the sterile neutrino is proportional to its mass. It gives a large energy density and it is constrained strongly. For the case of $m_{\nu_{\rm s}} \geq 1\,{\rm MeV}$, there are no allowed parameter region consistent with the 2 σ limit from observational data.

We showed a result of a parameter search in the plane of (θ, $m_{\nu_{\rm s}}$) for a fixed $E_{\rm res}$ value. We found that the region of a large mass and a large mixing angle is excluded. The heavier mass leads to a larger energy density, and the larger mixing angle leads to a later decoupling and a larger number density. In both cases, the energy density is larger, and that parameter region is constrained (Fig. 11). We also showd a result of a parameter search in the plane of ($E_{\rm res}$, $m_{\nu_{\rm s}}$) for a fixed θ value. We then checked trends of large effects for larger mass and the characteristic resonance energy (Fig. 12).

ACKNOWLEDGMENTS

This work is supported by the National Research Foundation of Korea (Grant No. NRF-2014R1A2A2A05003548 and NRF-2015K2A9A1A06046598). MK is supported by JSPS Postdoctoral Fellowship for Research Abroad.

[1] A. Aguilar-Arevalo *et al.* [LSND Collaboration], Phys. Rev. D **64**, 112007 (2001)
[2] A. A. Aguilar-Arevalo *et al.* [MiniBooNE Collaboration], Phys. Rev. Lett. **105**, 181801 (2010)
[3] B. Bhattacharya, R. J. Hill and G. Paz, Phys. Rev. D **84**, 073006 (2011)
[4] C. Giunti and M. Laveder, Phys. Rev. C **83**, 065504 (2011)
[5] M. G. Aartsen *et al.* [IceCube Collaboration], Phys. Rev. Lett. **117**, no. 7, 071801 (2016)
[6] H. Päs, S. Pakvasa and T. J. Weiler, Phys. Rev. D **72**, 095017 (2005)
[7] N. Arkani-Hamed, S. Dimopoulos and G. R. Dvali, Phys. Lett. B **429**, 263 (1998); N. Arkani-Hamed, S. Dimopoulos and G. R. Dvali, Phys. Rev. D **59**, 086004 (1999); I. Antoniadis, N. Arkani-Hamed, S. Dimopoulos and G. R. Dvali, Phys. Lett. B **436**, 257 (1998)
[8] G. Shiu and S. H. H. Tye, Phys. Rev. D **58**, 106007 (1998) doi:10.1103/PhysRevD.58.106007 [hep-th/9805157].
[9] L. Randall and R. Sundrum, Phys. Rev. Lett. **83**, 3370 (1999)
[10] L. Randall and R. Sundrum, Phys. Rev. Lett. **83**, 4690 (1999)
[11] E. Aeikens, H. Päs, S. Pakvasa and T. J. Weiler, arXiv:1606.06695 [hep-ph].
[12] M. Kusakabe *et al.*, Phys. Rev D **93**, 043511 (2016).
[13] M. Kusakabe, K. S. Kim, M-K. Cheoun, T. Kajino, Y. Kino and J. Mathews, Astrophys. J. Suppl. **214**, 1 (2014).
[14] K. Ichiki, M. Yahiro, T. Kajino, M. Orito and G. J. Mathews, Phys. Rev. D **66**, 043521 (2002) doi:10.1103/PhysRevD.66.043521 [astro-ph/0203272].
[15] N. Sasankan, M. R. Gangopadhyay, G. J. Mathews and M. Kusakabe, arXiv:1607.06858 [astro-ph.CO].
[16] B. W. Lee and S. Weinberg, Phys. Rev. Lett. **39**, 165 (1977). doi:10.1103/PhysRevLett.39.165
[17] K. Sato and M. Kobayashi, Prog. Theor. Phys. **58**, 1775 (1977). doi:10.1143/PTP.58.1775
[18] P. Binetruy, C. Deffayet, U. Ellwanger and D. Langlois, Phys. Lett. B **477**, 285 (2000)
[19] C. Csaki, M. Graesser, C. F. Kolda and J. Terning, Phys. Lett. B **462**, 34 (1999)
[20] J. M. Cline, C. Grojean and G. Servant, Phys. Rev. Lett. **83**, 4245 (1999)
[21] R. Cooke, M. Pettinin, R. A. Jorgenson, M. T. Murphy and C. C. Steidel, Astrophys. J. **781**, 31 (2014)
[22] Y. I. I.Zotov, T.X. Thuan and N. G. Guserva, Mon. Not. ROy. Astron. Soc. **445**, 778
[23] E.W. Kolb and M.S. Turner, The early universe (westview press, 1994), Chap. 5
[24] R. Barbieri and A. Dolgov, Phys. Lett. B **237**, 440 (1990); R. Barbieri and A. Dolgov, Nucl. Phys. B **349**, 743 (1991).
[25] K. Enqvist, K. Kainulainen and M. J. Thomson, Nucl. Phys. B **373**, 498 (1992).
[26] A. D. Dolgov, S. H. Hansen, G. Raffelt and D. V. Semikoz, Nucl. Phys. B **580**, 331 (2000)
[27] L. Wolfenstein, Phys. Rev. D **17**, 2369 (1978).
[28] S. P. Mikheev and A. Y. Smirnov, Nuovo Cim. C **9**, 17 (1986).
[29] H. Ishida, M. Kusakabe and H. Okada, Phys. Rev. D **90**, no. 8, 083519 (2014)
[30] L. Wolfenstein, Phys. Rev. D **17**, 2369 (1978); S.P. Mikheev and A. Y. Smirnov, Nuovo Cimento Soc. Ital.

Fis. C **9**, 17 (1986); S. P. Mikheev and A. Y. Smirnov, Yad. Fiz. **42**, 1441 (1985)[Sov. J. Nucl. Phys. **42**, 913 (1985)]; V.D. Barger, K. Whisnant, S. Pakvasa, and R.J.N. Phillips, Phys. Rev. D **22**, 2718 (1980)

[31] P. Petreczky, J. Phys. G **39**, 093002 (2012)

[32] P. Descouvemont, A. Adahchour, C. Angulo, A. Coc and E. Vangioni-Flam, "Compilation and R-matrix analysis of Big Bang nuclear reaction rates," Atom. Data Nucl. Data Tabl. **88**, 203 (2004).

[33] A. Coc, P. Petitjean, J. P. Uzan, E. Vangioni, P. Descouvemont, C. Iliadis and R. Longland, "New reaction rates for improved primordial D/H calculation and the cosmic evolution of deuterium," Phys. Rev. D **92**, no. 12, 123526 (2015) doi:10.1103/PhysRevD.92.123526.

[34] L. Kawano, NASA STI/Recon Technical Report N **92** 25163 (1992).

[35] M. S. Smith, L. H. Kawano and R. A. Malaney, "Experimental, computational, and observational analysis of primordial nucleosynthesis," Astrophys. J. Suppl. **85**, 219 (1993).

[36] K. A. Olive *et al.* [Particle Data Group Collaboration], "Review of Particle Physics," Chin. Phys. C **38**, 090001 (2014).

[37] P. A. R. Ade *et al.* [Planck Collaboration], "Planck 2013 results. XVI. Cosmological parameters," Astron. Astrophys. **571**, A16 (2014).